Nuclear Materials and Energy 19 (2019) 189–194

Contents lists available at ScienceDirect

Nuclear Materials and Energy

journal homepage: www.elsevier.com/locate/nme

Interdiffusion and phase formation at iron-tungsten interfaces

Maximilian Reisner[*,a,b], Martin Oberkofler[a], Stefan Elgeti[a], Martin Balden[a], Till Höschen[a], Matej Mayer[a], Tiago F. Silva[c]

[a] Max Planck Institut für Plasmaphysik, Boltzmannstr. 2, Garching 85748, Germany
[b] Technische Universität München, Garching, Germany
[c] Instituto de Física da Universidade de São Paulo, Rua do Mãtao, trav. R 187, São Paulo 05508-090, Brazil

ARTICLE INFO

Keywords:
Diffusion
Iron
Tungsten
Rutherford backscattering spectrometry
X-Ray photoelectron spectroscopy
Eurofer

ABSTRACT

Low-activation steels are attractive candidates for wall materials in future nuclear-fusion power plants. Through a process called preferential sputtering, an enriched tungsten (W) layer is expected to develop on these steels, lowering erosion and thus increasing their lifetime and reducing contamination of the fusion plasma. However, the process of preferential sputtering may be counteracted by interdiffusion of W and iron (Fe). In this article, we investigate a simplified model system of such low-activation steels with a W-rich layer on the surface, by sputter depositing a thin W layer on top of pure Fe substrates. We investigate the processes that are activated when this model system is subject to temperatures relevant in the context of nuclear fusion reactors and assess the temperatures at which interdiffusion is expected to influence W surface concentrations. This is done by annealing a binary W-Fe system and analyzing the resulting concentration profiles by means of Rutherford backscattering spectrometry (RBS) and focused ion beam cross-sectioning (FIB). For annealing temperatures above 1000 K, an intermediate phase was observed to have formed, both between the Fe and W layer as well as on the surface of the W layer. This intermediate phase was determined to be Fe_2W using Sputter X-ray photoelectron spectroscopy (XPS) and time-of-flight Rutherford backscattering spectrometry (ToF-RBS). The laterally averaged growth rate of this phase was determined to be $(1.0 \pm 0.1) \times 10^{-18} \frac{m^2}{s}$ at 1050 K and $(2.8 \pm 0.2) \times 10^{-18} \frac{m^2}{s}$ at 1100 K.

1. Introduction

Low-activation steels are attractive candidates for first-wall materials in certain recessed areas of the first wall of future nuclear-fusion power plants [1]. Through preferential sputtering of the lighter constituents, an enriched W layer is expected to develop on these steels, lowering erosion and thus increasing their lifetime and reducing contamination of the fusion plasma [2–4]. However, the process of W enrichment may be counteracted by interdiffusion of W and Fe, especially at elevated temperatures [5–7]. In order to predict the performance of the material, simulations using SDTrimSP have previously been performed, taking preferential sputtering and diffusion into account [8]. These simulations require knowledge of the interdiffusion coefficient between Fe and W. Previous investigations of the diffusion of W in Fe were performed for W concentrations below 3 at% [9] or in the W tracer limit [10,11]. At the fusion reactor first wall, very high W concentrations (ideally close to 100 at%) would be desirable. We are, therefore, interested in the interdiffusion of Fe and W throughout the entire concentration range. The W-Fe phase diagram [12] features the intermetallic phases FeW and Fe_2W. Since these phases could in principle also form at temperatures expected inside future nuclear-fusion reactors, the interdiffusion within these phases is also of interest, as well as the rate of phase growth at W-Fe interfaces.

After the description of the experimental procedure in Section 2 we investigate the phase growth at Fe-W interfaces in Section 3. In Section 4 we show that this newly formed intermediate phase is in fact Fe_2W. Finally, in Section 5 we use Rutherford backscattering spectrometry (RBS) to qualitatively assess the degree of interdiffusion and to get estimates of the effect of elevated W concentrations on the interdiffusion of Fe and W by comparing the available literature values for low W concentrations.

2. Experimental

2.1. Sample preparation

Substrates of 99.99+ wt% (Goodfellow FE000411) and 99.5 wt% pure iron (Goodfellow FE000410) were polished to R_a roughness values

* Corresponding author.
E-mail address: maximilian.reisner@ipp.mpg.de (M. Reisner).

https://doi.org/10.1016/j.nme.2019.01.033
Received 24 September 2018; Received in revised form 18 January 2019; Accepted 22 January 2019
Available online 04 March 2019

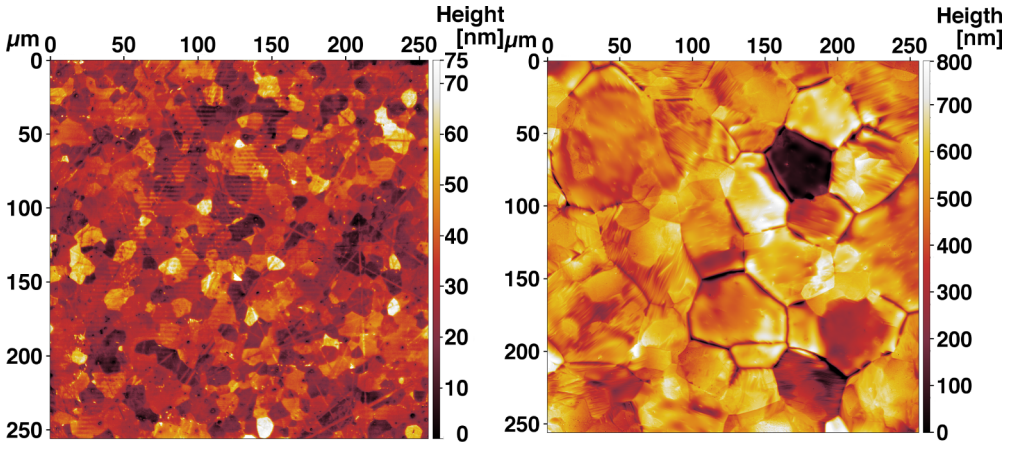

Fig. 1. Confocal laser scanning microscope images of a typical iron substrate after being polished (left) and after being annealed for 96 h at 1200 K. The average grain size grew from approximately 10 μm to 50 μm.

of 10 nm. The resulting amorphous deformation layer on the surface as well as the present grain boundaries with their high density of lattice defects can influence the diffusion processes. For a well-defined experiment addressing bulk interdiffusion, these influences need to be minimized. Therefore, subsequently to polishing, the samples were annealed in a vacuum ($\sim 10^{-6}$mbar) for 96 h at 1200 K to recrystallize the deformation layer induced by the polishing process and to induce grain growth. After annealing, the grains have grown to a size of approximately 50 μm (Fig. 1).

After polishing and annealing, a 1 μm thick W layer was deposited on the Fe substrates by magnetron sputtering. The resulting W-Fe couples were annealed in a vacuum at temperatures between 900 K and 1100 K and for times between 6 h and 60 h to induce diffusion and phase formation (see Table 1).

2.2. Analysis techniques

The width distributions of intermediate phases were determined with scanning electron microscopy (SEM). For this, cross-sections were cut with a focused Ga^+ ion beam. On these, images were taken, by collecting secondary electrons (SE) (see Section 3).

In order to determine the stoichiometry of the intermediate phase, X-ray photoelectron spectroscopy (XPS) spectra were acquired to analyze the near-surface composition of a sample annealed for 48 h at 1100 K using a PHI 5600 ESCA system equipped with an Al K_α X-ray source. The surface of this sample is completely covered by the intermediate phase. Depth profiling was performed by sputter-erosion using a beam of 10 keV Ar + ions at an incident angle of 20°, periodically eroding the surface and alternately recording the photoelectron spectra in a surface area of approximately 400 μm diameter. The concentration of W was determined from the 4f line, the concentration of Fe from the 2p line (see Section 4).

A further means to determine the stoichiometry, also described in Section 4, are the time-of-flight Rutherford backscattering spectrometry (ToF-RBS) measurements we performed in the newly built ToF ion beam analysis (ToF-IBA) apparatus [13] at the IPP Tandem accelerator using incident 5 MeV ^{28}Si ions at normal incidence. Backscattered particles were recorded at a scattering angle of 150° with a detector

Table 1
Overview of annealing times and temperatures and the applied analysis techniques (see Section 2.2). Cells highlighted in blue indicate samples where the formation of an intermediate phase was observed. Cells of which the content is bold and italic indicate an incompletely formed intermediate phase (see Section 3). Cells of which the content is underlined indicate that the Fe substrates with the inferior purity were used.

T [K] \ t [h]	6	12	24	36	48	51	60	200
900	RBS SEM			RBS			RBS SEM	
1000	RBS SEM	RBS	***RBS*** ***SEM***	***RBS*** ***SEM***			SEM	TOF
1050	RBS SEM	SEM	RBS SEM	RBS SEM	RBS SEM	RBS SEM		
1100	SEM	SEM	RBS SEM	SEM TOF	RBS SEM XPS TOF			

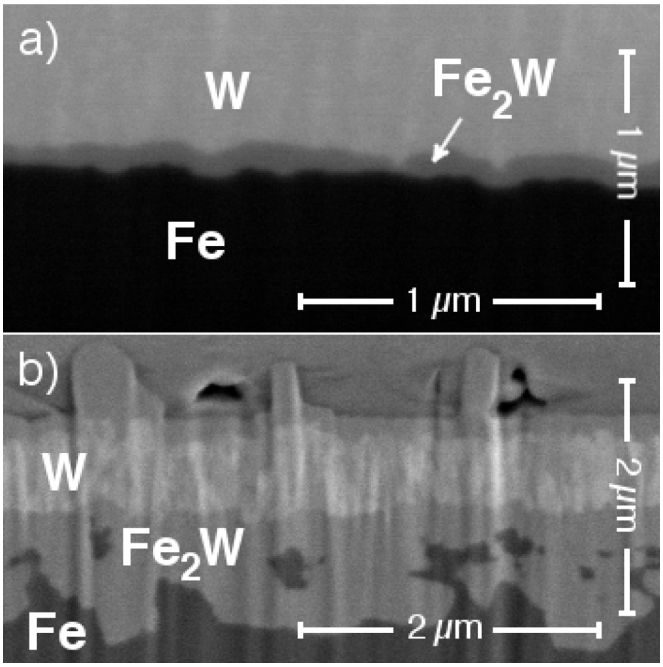

Fig. 2. SEM images of FIB cut cross-sections on samples heated for a) 12 h at 1050 K and b) 48 h at 1100 K. The cross-section plane and the image plane include an angle of 38°.

having a free flight path of 1.315 m, and a time resolution of 600 ps. The measured time spectra were converted to energy spectra, which were in turn converted to depth profiles using the simulation program SIMNRA [14]. The depth profiles in units of $\frac{\text{atoms}}{\text{cm}^2}$ are converted to nm by SIMNRA, based on the weighted atomic densities of pure W and Fe.

After annealing, on most samples depth profiles were measured with conventional RBS at the 3 MV Tandem accelerator of IPP, using ^{4}He ions with 4 and 6 MeV incident energy at incident angles of 0° and 45°. Backscattered particles were detected with a passivated implanted planar silicon (PIPS) detector at a scattering angle of 165° in Cornell geometry, having a solid angle of 1.097 ± 0.036 msr and a nominal energy resolution of 18 keV. The measured energy spectra were again converted to depth profiles using the simulation program SIMNRA [14]. (see Section 5.1) The footprint of the beam has a diameter of approximately 1 mm, resulting in the signal being a lateral average over this area.

3. Phase growth

Fe-W couples were systematically annealed under vacuum conditions for various times at temperatures between 900 and 1100 K. In these Fe-W couples, cross-sections of 30 μm to 100 μm length were cut with FIB and observed with SEM to see if an intermediate phase has formed. In the (SE) images, this phase is visible as an initially thin homogeneous band with a shade of grey in between the relatively bright W and the darker Fe (see for example Fig. 2). For 900 K, no phase formation is observed after annealing times of up to 60 h. At 1000 K, we observe an intermediate phase in isolated nucleation sites after 24 h of annealing. After 60 h then, the intermediate phase is fully formed between the Fe and the W. At 1050 K and 1100 K, the fully formed intermediate phase was observed after 12 h of annealing (see Table 1). In Fig. 2, cross-sections of two samples annealed at 1050 K for 12 h and at 1100 K for 24 h are shown.

To extract lateral thickness distributions of the intermediate phases from such SEM images, at every horizontal position, the pixels colored in the intermediate shade of grey were manually marked and then each column of pixels was summed up vertically. By multiplication of the resulting number of pixels with the pixel height, width profiles along the cross-sections were obtained. Regions, where obviously bulk interdiffusion was not the dominant process, i.e. where there is a channel of the intermediate phase going through the W layer, were excluded. For more details on these processes see Section 4.

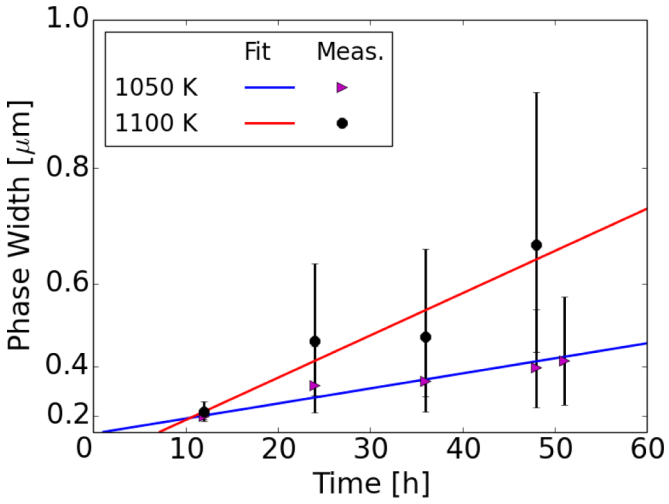

Fig. 3. Width of the intermediate phases vs annealing time at 1050 K and 1100 K. The scale of the y-axis is quadratic, so that the fitted square root dependences appear as straight lines.

The mean values and standard deviations of the resulting profiles are plotted in Fig. 3 as a function of annealing time for temperatures of 1050 and 1100 K. With increasing temperature and annealing time, the width of the intermediate phase grows and gets more irregular (Fig. 2).

In Fig. 3, it can be seen that the average width w grows with the square root of the time. From a fit through the data, we can determine a growth rate coefficient K, according to $w = \sqrt{Kt}$. At 1050 K, its value is $(1.0 \pm 0.1) \times 10^{-18} \frac{m^2}{s}$, at 1100 K it is $(2.8 \pm 0.2) \times 10^{-18} \frac{m^2}{s}$.

Upon fitting these data with a square-root time dependence (Fig. 3), we allowed for a time offset, since we observe no phase formation within at least the first 6 h. This time delay is attributed to a nucleation effect.

Further evidence for a nucleation time before the phase formation sets in, stems from the aforementioned annealing series at 1000 K which does not show a continuos intermediate phase after 24 and 36 h. Only after 60 h of annealing at that temperature, a continuous band of the intermediate phase is observed, with a thickness of (420 ± 160) nm.

The growth of an intermediate phase β at the interface between the two (initially sharply separated) constituents α and γ of a diffusion couple can be addressed analytically, [15] yielding the following time dependence of the thickness of the intermediate phase w:

$$w = \sqrt{Kt} = \sqrt{4D^{\beta}(K^{\beta\alpha} - K^{\beta\gamma})^2 t}\,. \tag{1}$$

Here, D^{β} is the diffusion coefficient in the intermediate phase. The growth rate K is dependent on D^{β} as well as on the dimensionless proportionality factors $K^{\alpha\beta}$ and $K^{\beta\gamma}$, that are themselves implicitly dependent on the solubility ranges and the diffusion coefficients of the individual phases. This analytical formula is valid under the assumptions of a semi-infinite diffusion couple, a flat interface and in the case where interdiffusion is controlled by volume diffusion (interface diffusion and phase formation being fast and therefore negligible). Furthermore, any concentration dependence of the diffusion coefficient within each phase is assumed to be negligible.

Even though we only have a thin layer of W, the assumption of a semi-infinite diffusion couple is approximately true as long as there is a W layer remaining. The assumption of a flat interface, however, does not hold true, since the interface forms three dimensional structures.

Table 2
The interdiffusion coefficients in the Fe_2W phase (right column) along with the ranges for D_{Fe} and D_W used for their calculation. D_{Fe} was taken from available literature ([9],[10], and [11]), D_W was estimated based on the results from the RBS analyses described in Section 5.

T [K]	D_{Fe} [$10^{-19}\frac{m^2}{s}$]	D_W [$10^{-19}\frac{m^2}{s}$]	D_{Fe_2W} [$10^{-19}\frac{m^2}{s}$]
1050	500 – 1200	0.05 – 5	13.5 ± 0.5
1100	1000 – 10,000	0.1 – 10	42 ± 7

Nonetheless, we apply Eq. 1 to our data, to get an estimate of the interdiffusion coefficient between Fe and W at larger concentrations of W. The results of this analysis can be seen in Table 2.

For this analysis, we require the solubility ranges of the pure W and Fe phases, as well as the solubility range of the intermediate phase itself. The solubility ranges of the pure phases, which also influence the growth coefficient K, can be taken from the literature and lie in the range of $0-1$ at.% W in case of the Fe phase and $99.5-100$ at.% W in case of the W phase [12]. For the solubility range of the intermediate phase, we chose to use a range of $28-38$ at.% W, which is a 5 % point variation around 33 at.% W, the concentration of Fe_2W. It will be shown in Section 4 that this is the intermediate phase we observe. The range of 5 % is supported by depth profiles extracted from energy-dispersive X-ray emission maps of the FIB cross-sections (data not shown) as well as by ToF-RBS measurements (see Section 4)

Additionally, we need the interdiffusion coefficients in the original phases of the diffusion couple, which in our case are the tracer diffusion coefficients. For the diffusion coefficient within the pure Fe phase D_{Fe}, literature values are available ([9–11]). The diffusion coefficient within the pure W phase D_W we approximate based on the values estimated from RBS (see Section 5.2). Such a very rough estimation can be accepted because the diffusion coefficients of the pure phases have a much smaller influence on K compared to the diffusion coefficient of the intermediate phase D_{Fe_2W} [15].

4. Stoichiometry of the intermediate phase

For samples annealed at 1000 K and above, we observe discontinuations or gaps in the W layer, which are filled by the intermediate phase. Furthermore, the intermediate phase extends towards the surface of the substrate. This occurs primarily (however not exclusively) at grain boundaries of the Fe substrate. This enhanced formation of the intermediate phase inside grain boundaries and the subsequent spreading of the intermediate phase on the surface could be explained by grain boundary effects such as grain boundary wetting and segregation [16]. Though we would like to point out that the temperatures at which we anneal our binary Fe/W system are well below the melting temperatures of Fe and W, which makes grain boundary wetting effects, such as reported in e.g. [17] or [18], unlikely.

The phase at the surface has the same shade of grey in SEM-images as the phase that develops at the Fe-W interface (see Fig. 4). EDX measurements confirm a homogeneous Fe/W ratio within this phase.

Determination of the stoichiometry of this phase from the EDX measurements requires some rather sophisticated analysis of the data including background subtraction and modeling of the physical processes involved in the signal generation (penetration and stopping of electrons, energy-dependent excitation, etc.). A quantification of the stoichiometry has been attempted on images acquired at two different microscopes with analytic software from different companies. The results for the stoichiometry were in the range from 40 % to 53 % W for one microscope and in the range from 71 % to 80 % W for the other, and therefore inconclusive.

We were able to take advantage of this intermediate phase formation at the surface by employing very surface sensitive analysis techniques, namely sputter-XPS and ToF-RBS to determine the composition

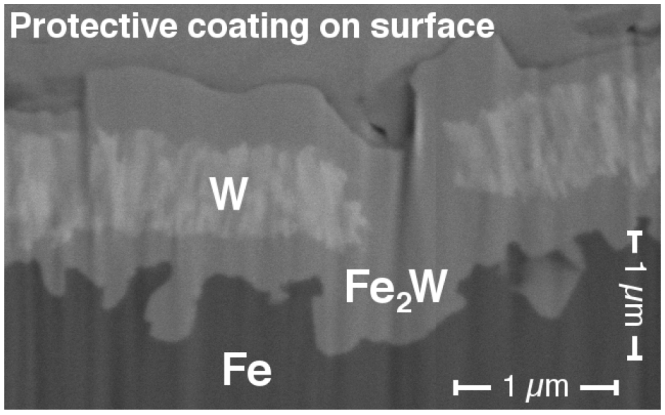

Fig. 4. Cross-section SEM image of a FIB cut showing a crack in the W layer with the intermediate phase at the Fe-W interface, within the crack and on top of the W layer. Image taken on a sample annealed for 24 h at 1100 K. Angle between cross-section and view plane include an angle of 38°.

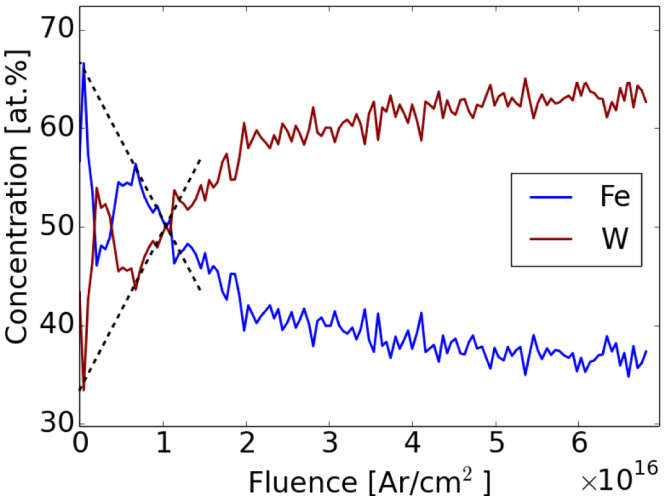

Fig. 5. Sputter-XPS depth profile of the intermediate phase on a sample heated for 48 h at 1100 K. The sum of the sensitivity-weighted signals from the W 4f and the Fe 2p line emission is normalized to one and the contributions are plotted vs the applied Ar-fluence. The dashed lines are drawn to guide the eye and indicate the extrapolation of the concentrations towards the surface.

of the intermediate phase.

Sputter-XPS analysis was performed on the surface of a substrate annealed for 48 h at 1100 K. These annealing conditions lead to a complete coverage of the W surface by the intermediate phase. This is necessary, because XPS has no lateral resolution and averages over the whole analysis region of approximately 400 μm diameter. The depth profile determined by sputter-XPS is shown in Fig. 5. Since there are impurities such as C and O adsorbed to the surface of the sample, due to exposure to air, and because the sputter-XPS analysis alters the stoichiometry of our sample through preferential sputtering, we have to extrapolate the depth profile back to the original surface of the substrate to determine the stoichiometry present before the onset of Ar bombardment and before surface oxidation. This extrapolation suggests a Fe:W ratio of 2:1, indicating that the intermediate phase formed is Fe_2W.

Complementarily to this extrapolation from sputter-XPS measurements, the near-surface layer was additionally examined using high-resolution ToF-RBS. Depth profiles resulting from the analysis of three different samples (of which one was also analysed by XPS) that were heated for sufficiently long times and at sufficiently high temperatures to ensure that their surface is completely covered with the intermediate

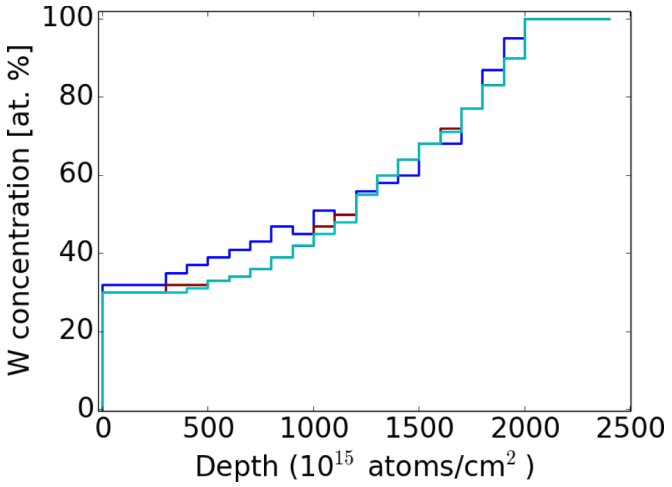

Fig. 6. Depth profiles extracted from ToF-RBS analyses of the surfaces of three samples that were annealed for 200 h at 1000 K (blue) and for 36 (red) and 48 h (cyan) at 1100 K and so that their entire surface is covered by the intermediate phase. To give a rough estimate of the actual thickness of the Fe_2W layer: based on the density of pure W of 19.29 $\frac{g}{cm^3}$, $10^{15}\frac{atoms}{cm^2}$ is equivalent to 0.158 nm. (For interpretation of the references to color in this figure legend, the reader is referred to the web version of this article.)

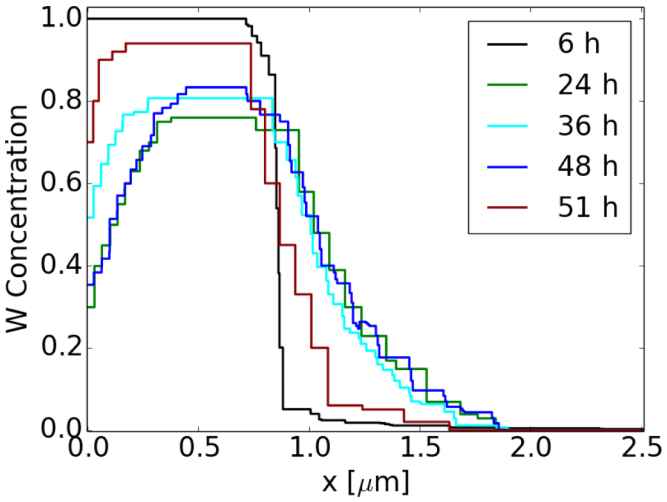

Fig. 7. Concentration profiles obtained from RBS, from samples heated at 1050 K. The sample that was heated for 51 h had a Fe substrate of inferior purity.

phase, are shown in Fig. 6. At a depth of 2×10^{18} atoms/cm^2 the W concentration approaches 100 %, which is consistent with the thickness of the intermediate phase on top of the underlying W layer as visible in FIB cross-sections, cf. Fig. 2. The analysis depth is limited to the plotted region because at larger depths the interpretation of the ToF-RBS signal is compromised by the increasing influence of multiple scattering. The measured W concentration in the top 50 nm is 30 - 32 at. %. Taking the uncertainties of about 10 % of this method into account, this result is consistent with the assumption of Fe_2W. We, therefore, conclude that the intermediate phase is most likely the metastable phase Fe_2W.

5. Analysis using Rutherford backscattering spectrometry

In addition to the analysis of FIB cross-sections described in Section 3, we also pursued a complementary approach to characterize the behavior of our Fe-W model system under high temperatures, namely by means of RBS. This analysis technique features a suitable information depth and depth resolution for the assessment of elemental depth profiles in the prepared samples. However, due to the size of the analysis spot, the resulting profiles are laterally averaged over roughly 1 mm^2. Due to the inhomogeneous growth of the intermediate phase, apparent e.g. in Fig. 2, this lateral averaging is going to yield continuous depth profiles. Each concentration value corresponds to the average concentration at a given depth. Because of this lateral averaging, the Fe_2W phase we observed with SEM does not appear in the depth profiles obtained via RBS.

In this section, we use these averaged depth profiles to determine at which temperatures diffusion effects become relevant. Furthermore, based on these averaged depth profiles, we estimate 'apparent' concentration dependent diffusion coefficients.

Since these coefficients are only based on laterally averaged data, which do not resolve the observed phase formation and neglects the inhomogeneous growth, its physics basis is obviously flawed and the obtained coefficients cannot fully be depended on. Also, since the sputter deposited W layer consists likely out of small grains, increased transport through W/W grain boundaries cannot be ruled out, which could add a significant contribution to the bulk diffusion. Studying such possible grain boundary effects and their underlying mechanisms, however, was beyond the scope of this work.

Nonetheless, these apparent diffusion coefficients allow us to get an idea of how the interdiffusion coefficient between Fe and W behaves at higher concentrations of W, at least in systems where a thin layer of W is present on top of a Fe substrate, which is relevant for the study of low-activation steels in future nuclear-fusion power plants. And assuming that the W-rich layers on these steels, resulting from preferential sputtering, also feature small grains, our 'apparent diffusion coefficients' would be an accurate representation of the rate at which W diffuses away from the W enriched layer.

5.1. Depth profiles from RBS analysis

Fig. 7 shows typical W concentration depth profiles obtained from RBS measurements with the aid of the simulation code SIMNRA.

It should again be noted, that due to the averaging over lateral inhomogeneities, these profiles are continuous, with concentrations spanning over all values between 0 and 1 and they do not feature discrete phases. After six h, the profile is already smeared out a little bit, while in reality the interface is still very sharp, as could be seen in the FIB cuts. This initial interface width therefore reflects the resolution of the RBS analysis. Going to longer annealing times, the interface becomes more and more smeared out.

As the Fe_2W phase forms and grows also on the surface (in addition to the interface) with longer annealing times, the W concentration does not reach 100 % anymore at the surface, and even decreases towards the surface. Upon annealing of a diffusion couple with the inferior substrate purity (the sample annealed for 51 h) we notice that the profile is much less smeared out and there is less Fe_2W at the surface. This indicates that impurity concentrations in the per mill range can have a considerable influence on the interdiffusion rates.

5.2. Apparent interdiffusion coefficients from RBS analysis

To obtain our 'apparent interdiffusion coefficients', a simple code was written, that can simulate one-dimensional diffusion-processes using concentration-dependent interdiffusion coefficients. These finite-difference simulations were implemented using the stable, second-order convergent Crank-Nicolson method [19]. This code is then run with varying diffusion coefficients D(c), to find the concentration dependence for which the difference between the measured and the simulated depth profiles is minimized. The simulations were benchmarked using the Boltzmann-Matano method [20]. Due to the low resolution of the measured data, obtaining the diffusion coefficients directly with the Boltzmann-Matano method was not possible.

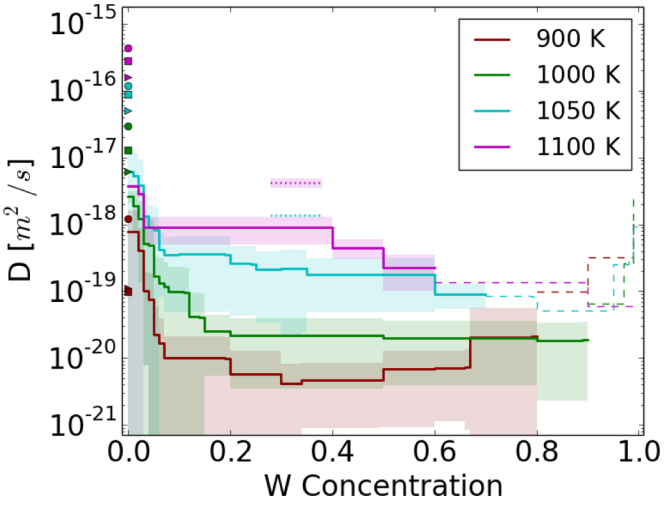

Fig. 8. Concentration dependence of the apparent interdiffusion coefficient for various temperatures. Shaded regions indicate the uncertainty of the values. The results for higher W concentrations were compromised by the appearance of Fe_2W on the surface, and can, therefore, not be relied upon. Thus, they are only shown as dashed lines. The dotted lines indicate the values estimated from the growth rate of the intermediate phase. Also displayed are the values from the literature, for comparison. The points indicated with circles are from [9], the points indicated with triagles are from [10] and the points indicated with squares are taken from [11].

At elevated temperatures, the concentration profiles close to the surface are dominated by the Fe_2W layer, whose development is influenced by the other processes than bulk diffusion alone. Therefore, regions of high W concentrations were excluded from the fits for these temperatures. As a result, it was not possible to estimate diffusion coefficients for very high W concentration values (see Fig. 8).

Since the diffusion coefficient is not time dependent, the resulting diffusion coefficients should be the same for different annealing times at a given temperature. Therefore, for each investigated temperature, an average over the resulting diffusion coefficients that result from the different samples annealed for different lengths of time is taken. The results are shown in Fig. 8. As error estimation, one standard deviation from this average was used.

We have to stress again that these 'apparent diffusion coefficients' mostly serve as a means to quantify our observations regarding the behavior of a thin W layer on a Fe substrate when being exposed to fusion reactor relevant temperatures. Yet still, these data allow us to get a general idea of the diffusion rates at intermediate concentrations of W. As can be seen in Fig. 8, it appears that the diffusion coefficients quickly decrease by approximately one or two orders of magnitude towards higher concentrations of W compared to the values at the tracer limit, which are in general agreement with the existing literature values. As could be expected, higher temperatures lead to higher diffusion coefficients.

6. Summary and conclusions

In this paper, we studied the interdiffusion and phase formation at Fe-W interfaces.

SEM images were acquired after annealing, on cross-sections that were cut into the material surfaces by focused ion beam milling. For annealing temperatures above 1000 K, the formation of an intermediate phase was observed. The stoichiometry resulting from XPS and ToF-RBS measurements is consistent with the known metastable phase Fe_2W. The laterally averaged growth rate K of this phase was found to be $(1.0 \pm 0.1) \times 10^{-18} \frac{m^2}{s}$ at 1050 K, and $(2.8 \pm 0.2) \times 10^{-18} \frac{m^2}{s}$ at 1100 K.

From RBS measurements, laterally averaged depth profiles could be obtained for temperatures between 900 and 1100 K. From these, 'apparent diffusion coefficients' could be estimated, which suggest that the diffusion between W and Fe is strongly reduced for concentrations far beyond the W tracer limit. While the exact values we obtained might be skewed by grain boundary effects, the general trend is rather clear. This reduced diffusion would be a favourable behavior for low activation steels like EUROFER, at the surface of which a W-enriched layer is expected to form due to preferential sputtering. This would increase the potential for application of low-activation steels as first-wall materials.

Acknowledgments

This work has been carried out within the framework of the EUROfusion Consortium and has received funding from the Euratom research and training programme 2014–2018 under grant agreement No. 633053. The views and opinions expressed herein do not necessarily reflect those of the European Commission. Work was performed under EUROfusion WP PFC.

References

[1] H. Bolt, et al., Plasma facing and high heat flux materials – needs for ITER and beyond, J. Nucl. Mater. 307 (2002) 43–52.
[2] J. Roth, et al., EUROFER as wall material: reduced sputtering yields due to W surface enrichment, J. Nucl. Mater. 454 (1–3) (2014) 1–6, https://doi.org/10.1016/j.jnucmat.2014.07.042.
[3] K. Sugiyama, et al., Erosion of EUROFER steel by mass-selected deuterium ion bombardment, Nucl. Mater. and Energy 16 (2018) 114–122.
[4] K. Sugiyama, et al., Erosion study of Fe–W binary mixed layer prepared as model system for RAFM steel, J. Nucl. Mater. 463 (2015) 272–275, https://doi.org/10.1016/j.jnucmat.2014.11.044.
[5] V. Alimov, et al., Surface modification and sputtering erosion of reduced activation ferritic martensitic steel F82h exposed to low-energy, high flux deuterium plasma, Nucl. Mater. and Energy 7 (2016) 25–32, https://doi.org/10.1016/j.nme.2016.01.001.
[6] M. Balden, et al., Effect of the surface temperature on surface morphology, deuterium retention and erosion of EUROFER steel exposed to low-energy, high-flux deuterium plasma, Nucl. Mater. and Energy 12 (2017) 289–296, https://doi.org/10.1016/j.nme.2017.01.001.
[7] H. Koslowski, et al., Temperature-dependent in-situ LEIS measurement of W surface enrichment by 250 eV D sputtering of EUROFER, Nuclear Materials and Energy 16 (2018) 181–190, https://doi.org/10.1016/j.nme.2018.07.001.
[8] U.v. Toussaint, et al., Simulation of coupled sputter-diffusion effects, Phys. Scr. T167 (2016) 014023, https://doi.org/10.1088/0031-8949/T167/1/014023.
[9] P.J. Alberry, C.W. Haworth, Interdiffusion of Cr, Mo, and W in iron, Metal Science 8 (1) (1974) 407–412.
[10] R.A. Pérez, D.N. Torres, W diffusion in paramagnetic and ferromagnetic α-Fe, Appl. Phys. A 104 (1) (2011) 329–333, https://doi.org/10.1007/s00339-010-6142-x.
[11] S. Takemoto, et al., Diffusion of tungsten in α-iron, Philos. Mag. 87 (11) (2007) 1619–1629, https://doi.org/10.1080/14786430600732093.
[12] O. Madelung (Ed.), Dy-Er Fr-Mo, Landolt-Börnstein - Group IV Physical Chemistry, vol. E, Springer-Verlag, Berlin/Heidelberg, 1995, doi:10.1007/b55397.
[13] M. Mayer, et al., Tungsten surface enrichment in EUROFER and Fe-W model systems studied by high-resolution time-of-flight rutherford backscattering spectroscopy, Nucl. Mater. Energy 17 (2018) 147–151, https://doi.org/10.1016/j.nme.2018.10.004.
[14] M. Mayer, Simnra, a simulation program for the analysis of NRA, RBS and ERDA, AIP Conf. Proc. 475 (1) (1999) 541–544, https://doi.org/10.1063/1.59188.
[15] M. Kajihara, Analysis of kinetics of reactive diffusion in a hypothetical binary system, Acta Mater. 52 (5) (2004) 1193–1200, https://doi.org/10.1016/j.actamat.2003.10.047.
[16] A. Vilenkin, Grain boundary segregation and grain boundary wetting, Defect Diffu. Forum 216–217 (2003) 189–196, https://doi.org/10.4028/www.scientific.net/DDF.216-217.189.
[17] A.B. Straumal, et al., Apparently complete grain boundary wetting in Cu–In alloys, J. Mater. Sci. 47 (24) (2012) 8336–8343, https://doi.org/10.1007/s10853-012-6773-8.
[18] B. Straumal, et al., Pseudopartial wetting of WC/WC grain boundaries in cemented carbides, Mater. Lett. 147 (2015) 105–108, https://doi.org/10.1016/j.matlet.2015.02.029.
[19] R.J. LeVeque, Finite Difference Methods for Ordinary and Partial Differential Equations: Steady-State and Time-Dependent Problems, SIAM, Philadelphia, PA, 2007. OCLC: ocm86110147.
[20] H. Mehrer, Diffusion in Solids Fundamentals, Methods, Materials, Diffusion-Controlled Processes, Springer, Berlin; New York, 2007. OCLC: 915958622.